 doi:10.20944/preprints202012.0045.v1

Article

Development of a Resolver-to-Digital Converter based on Second-Order Difference Generalized Predictive Control †

Thyago Estrabis, Gabriel Gentil and Raymundo Cordero

Graduation Program in Electrical Engineering, Federal University of Mato Grosso do Sul, Campo Grande, MS, Brazil; thyago.estrabis@gmail.com (T.E.); gabrielgent@gmail.com (G.G.); raymundo.garcia@ufms.br (R.C.)

* Correspondence: thyago.estrabis@gmail.com; Tel.: (+55 67 99333-2171)

† This paper is an extended version of "Application of Model Predictive Control in a Resolver-to-Digital Converter" published in Proceeding of the 2019 IEEE 15th Brazilian Power Electronics Conference and 5th IEEE Southern Power Electronics Conference (COBEP/SPEC) on Santos, SP, Brazil, 1–4 December 2019.

Abstract: High-performance motor drives that operate in harsh conditions require an accurate and robust angular position measurement to properly estimate the speed and reduce the torque ripple produced by angular estimation error. For that reason, a resolver is used in motor drives as a position sensor due to its robustness. A resolver-to-digital converter (RDC) is an observer used to get the angular position from the resolver signals. Most RDCs are based on angle tracking observers (ATOs). On the other hand, generalized predictive control (GPC) has become a powerful tool in the development of controllers and observers for industrial applications. However, no GPC-based RDC with zero steady-state error during constant speed operation was proposed. This paper proposes an RDC based on a second-order difference GPC (SOD-GPC). In SOD-GPC, the second order difference operator is applied to design a GPC model with two embedded integrators. Thus, the SOD-GPC is used to design a type-II ATO whose steady-state angle estimation error tends to zero during constant speed operation. Simulation and experimental results prove that the proposed RDC system has better performance than other approaches in literature.

Keywords: angle tracking observer, generalized predictive control, resolver, resolver-to-digital converter, tracking.

1. Introduction

High-performance applications based on electrical motors drives, such as electric/hybrid vehicles (EV/HEVs), aircraft, CNCs, and robotics, work under harsh conditions [1–3]. In those applications, an accurate motor shaft angular position measurement is required to get the angular speed and to perform vector control techniques [4–6]. Besides, a high error in the angular position estimation produces a high torque ripple that may lead to motor drive malfunctions [6]. Hence, a robust angular position sensor is required to guarantee the motor drive performance and reliability.

Encoder and resolver are the most used angular position sensors in industry [7–10]. Resolver is most used for harsh applications as it can resist higher temperatures, shocks, and vibrations than encoders [9,10]. A resolver generates two amplitude-modulated output voltages. For that reason, getting an angular position from resolver signals is a difficult task. Observers called resolver-to-digital converters (RDC) are used to estimate the angular position from the resolver outputs. Many RDCs were proposed in literature [11–18]. These approaches can be divided into open-loop RDCs and closed-loop RDCs. Closed-loop RDCs are more robust to noise and are usually based on an angle tracking observer (ATO): a closed-loop estimator that reduces the difference between the actual and the estimated angular position [13–18].

Preprints (www.preprints.org) | NOT PEER-REVIEWED | Posted: 2 December 2020 doi:10.20944/preprints202012.0045.v1

On the other hand, model predictive control (MPC) becomes an interesting research topic due to its fast response and robustness [19–22]. In the '60s, the modern control theory began to diffuse by the need to control more complex plants [23]. Interest in MPC begins in the late 1970s with the emergence of several papers and consolidating MPC in the industry [24]. This interest existed for his behavior in the time domain, and its robustness since the industrial engineers tend to use robust control [22]. Clarke, in [25,26], presented a generalized predictive control (GPC) model, one of MPC's robust methods [21]. The objective of GPC is to calculate a sequence of future control signals that minimize a cost function that represents the system performance [21,22]. That cost function is defined over a prediction window (a set of predicted plant responses). An augmented model of the plant is used to predict the plant responses. In recent works, predictive control is applied in driving systems [27–29], microgrids [30–32], HVAC systems [33,34], and other applications.

In [35], it was proposed for the first time the application of the conventional GPC described in [22] in the development of an ATO. In that approach, the ATO was modelled as a tracking system where the reference is the actual angular position and the system output is the estimated angle. Thus, the angle estimation is represented as a tracking problem. However, the ATO proposed in [35] has a steady-state angle estimation error during constant speed operation. In order to explain this error, let define $R(s)$, $G(s)$ and $C(s)$ be, respectively, the transfer function of the reference, the plant transfer function and the controller. According to the internal model principle, if the product $G(s)C(s)$ contains $R(s)$, then the plant output will asymptotically track the reference [36]. The angular position during constant speed operation is modeled as a ramp signal ($\theta(t) = \omega t$). Besides, the Laplace transform of a ramp signal is $1/s^2$. However, the conventional GPC system used in [35] has only one embedded integrator ($1/s$). Furthermore, the GPC cost function used in [35] considers that the reference signal is constant for the predicted outputs, which is false when the reference is a ramp signal. As a result, the ATO in [35] has an estimation error during constant speed operation.

Adaptations of GPC for ramp reference tracking were proposed [37–39]. Most of them require information about the reference and the solution of their cost functions to get their control law is not straightforward. However, in [39] is proposed a simple adaptation of the conventional GPC described in [22] for ramp reference tracking. That approach applies the second-order difference operator in order to create an augmented prediction model with two embedded integrators. Thus, according to the internal model principle, the GPC approach in [39] asymptotically tracks ramp references. Besides, the prediction window in [39] is composed by the predicted tracking errors. Due to the desired value of an error is always zero, then the prediction window reference vector is a set of zeros (i.e., a constant reference). Thus, the optimization and the receding horizon techniques used in [22] can be used to get the control law for ramp reference tracking. In this paper, in order to simplify the notation, the GPC approach described in [39] is called as second-order difference generalized predictive control (SOD-GPC).

In order to develop an ATO with the advantages of the GPC and with a zero steady-state angle estimation error during constant speed operation, this paper proposes an ATO based on the second-order difference generalized predictive control (SOD-GPC) described in [39]. As in [35], the ATO is modelled as a tracking system whose reference is the actual angular position and whose output is the estimated angle. During constant speed operation, the angular position (the reference) is a ramp signal. Thus, the SOD-GPC can be used for the angle estimation error to be asymptotically zero during constant speed operation.

The remainder of the paper is organized as follows. Section II describes the structure of the resolver and GPC. The proposed ATO is described in Section III. Simulation and experimental results shown in Section IV prove the good performance of the proposed ATO. Finally, conclusions are outlined. In this paper, $A \in \Re^{n \times m}$ denotes that A is a $n \times m$ matrix.

Preprints (www.preprints.org) | NOT PEER-REVIEWED | Posted: 2 December 2020 doi:10.20944/preprints202012.0045.v1

2. Theoretical Foundations

2.1. Resolver

Figure 1 shows the schematics of the resolver. It is composed by a excitation winding and two output windings. The excitation winding is coupled to the motor shaft and receives a sinusoidal excitation voltage $v_e(t)$ of several kHz (1-10 kHz) [11–18]:

$$v_e(t) = a_r cos(\omega_r t), \tag{1}$$

where a_r is the excitation voltage amplitude, $\omega_r = 2\pi f_r$ and f_r is the excitation voltage frequency. Two amplitude-modulated voltages $v_s(t)$ and $v_c(t)$ in the output windings. Those signals depend on the angular position [14]:

$$v_s(t) = k_r v_e(t) sin(\theta(t)), \tag{2}$$

$$v_c(t) = k_r v_e(t) cos(\theta(t)). \tag{3}$$

where $\theta(t)$ is the angular position to be measured, while k_r is the transformation ratio. The objective of a resolver-to-digital converter (RDC) is to get the angular position from $v_e(t)$, $v_s(t)$ and $v_c(t)$.

2.2. Difference Operation

Let $a(k)$ and $b(k)$ be discrete-time signals (vectors or scalars). The first-order difference operator (Δ) and the second-order difference operator (Δ^2) are defined as follows [40]:

$$\Delta a(k) = a(k) - a(k-1), \tag{4}$$

$$\Delta^2 a(k) = \Delta[\Delta a(k)] = \Delta a(k) - \Delta a(k-1). \tag{5}$$

Let M_1 and M_2 be matrices such as $M_1 a(k) + M_2 b(k)$ exists. The aforementioned operators are linear [39,40]:

$$\Delta[M_1 a(k) + M_2 b(k)] = M_1 \Delta a(k) + M_2 \Delta b(k), \tag{6}$$

$$\Delta^2[M_1 a(k) + M_2 b(k)] = M_1 \Delta^2 a(k) + M_2 \Delta^2 b(k). \tag{7}$$

The operator Δ corresponds to the discrete transfer function $C(z) = 1 - z^{-1}$ [22].

2.3. Conventional GPC

Consider that a n-order SISO (single-input single-output) plant has the following discrete-time space-state model:

$$x_m(k+1) = A_m x_m(k) + B_m u(k), \tag{8}$$

$$y(k) = C_m x_m(k), \tag{9}$$

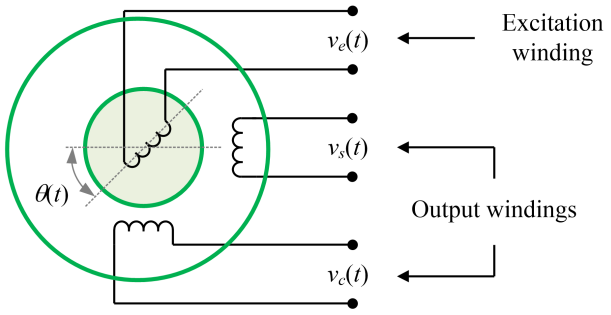

Figure 1. Schematic diagram of the resolver sensor.

Preprints (www.preprints.org) | NOT PEER-REVIEWED | Posted: 2 December 2020 doi:10.20944/preprints202012.0045.v1

where $u(k)$ is the plant input, $y(k)$ is the system output, $x_m(k) \in \Re^{n\times 1}$ is the plant state vector, while $A_m \in \Re^{n\times n}$, $B_m \in \Re^{n\times 1}$ and $C_m \in \Re^{1\times n}$. Let consider that the plant does not have an embedded integrator. The control system must have an integrator so that the steady-state error is zero for a step reference. Conventional GPC requires the development of an augmented model with an embedded integrator. This model will be used to predict the plant responses.

Applying the first-order difference operator (Δ) into (8) and (9), and based on (6), yields:

$$\begin{aligned} \Delta x_m(k+1) &= \Delta[A_m x_m(k) + B_m u(k)] \\ &= A_m \Delta x_m(k) + B_m \Delta u(k), \end{aligned} \tag{10}$$

$$\begin{aligned} \Delta y(k) &= \Delta[C_m x_m(k)] \\ &= C_m \Delta x_m(k), \end{aligned} \tag{11}$$

where

$$\Delta x_m(k) = x_m(k) - x_m(k-1), \tag{12}$$

$$\Delta x_m(k+1) = x_m(k+1) - x_m(k), \tag{13}$$

$$\Delta u(k) = u(k) - u(k-1), \tag{14}$$

$$\Delta y(k) = y(k) - y(k-1). \tag{15}$$

On the other hand, (16) can be proved based on (9), (15) and (10) [22]:

$$\begin{aligned} y(k+1) &= y(k) + \Delta y(k+1) \\ &= y(k) + C_m \Delta x_m(k+1) \\ &= y(k) + C_m A_m \Delta x_m(k) + C_m B_m \Delta u(k). \end{aligned} \tag{16}$$

The augmented model defined in (17) is obtained by placing (10) and (16) together in matrix form [22]:

$$\begin{aligned} \begin{bmatrix} \Delta x_m(k+1) \\ y(k+1) \end{bmatrix} &= \overbrace{\begin{bmatrix} A_m & o_m^T \\ C_m A_m & 1 \end{bmatrix}}^{\text{A}} \overbrace{\begin{bmatrix} \Delta x_m(k) \\ y(k) \end{bmatrix}}^{\text{x(k)}} + \overbrace{\begin{bmatrix} B_m \\ C_m B_m \end{bmatrix}}^{\text{B}} \Delta u(k) \\ y(k) &= \overbrace{\begin{bmatrix} o_m & 1 \end{bmatrix}}^{\text{C}} \overbrace{\begin{bmatrix} \Delta x_m(k) \\ y(k) \end{bmatrix}}^{\text{x(k)}}, \end{aligned} \tag{17}$$

where A, B and C, in 17 are the matrices of the augmented model, while $o_m \in \Re^{1\times n}$ vector composed of zeros. This augmented model allows predicting the plant responses. Consider that the state vector at the instant k_i, $x(k_i)$, is known. The future control trajectory is defined as:

$$\Delta u(k_i),\ \Delta u(k_i+1), \cdots,\ \Delta u(k_i+N_c-1), \tag{18}$$

where N_c is a variable called the control horizon. On the other hand, the future state variables are:

$$x(k_i+1|k_i),\ x(k_i+2|k_i), \cdots,\ x(k_i+N_p|k_i), \tag{19}$$

Preprints (www.preprints.org) | NOT PEER-REVIEWED | Posted: 2 December 2020 doi:10.20944/preprints202012.0045.v1

where $x(k_i+j|k_i)$ is the predicted state vector at instant k_i+j based on $x(k_i)$, while N_p is the prediction horizon, being $N_c \leq N_p$. The value of N_p defines the length of the prediction window [22]. In GPC, the future state variables are predicted using the control future trajectory and $x(k_i)$ [22]:

$$\begin{aligned} x(k_i+1|k_i) &= Ax(k_i) + B\Delta u(k_i), \\ x(k_i+2|k_i) &= A^2x(k_i) + AB\Delta u(k_i) + B\Delta u(k_i+1), \\ &\vdots \\ x(k_i+N_p|k_i) &= A^{N_p}x(k_i) + A^{N_p-1}B\Delta u(k_i) + \\ A^{N_pk-2}B\Delta u(k_i+1) &+ \cdots + A^{N_p-N_c}B\Delta u(k_i+N_c-1). \end{aligned} \tag{20}$$

As $y(k) = C_m x(k)$, the plant outputs are predicted based on (20):

$$\begin{aligned} y(k_i+1|k_i) &= CAx(k_i) + CB\Delta u(k_i), \\ y(k_i+2|k_i) &= CA^2x(k_i) + CAB\Delta u(k_i) + CB\Delta u(k_i+1), \\ &\vdots \\ y(k_i+N_p|k_i) &= CA^{N_p}x(k_i) + CA^{N_p-1}B\Delta u(k_i) + \\ CA^{N_p-2}B\Delta u(k_i+1) &+ \cdots + CA^{N_p-N_c}B\Delta u(k_i+N_c-1). \end{aligned} \tag{21}$$

Putting (21) into a matrix form, yields:

$$Y = Fx(k_i) + \phi U, \tag{22}$$

where $Y \in \Re^{N_p \times 1}$ is vector with the predicted responses, $U \in \Re^{N_c \times 1}$ is the vector with the future control actions, while F and ϕ are defined in (25) :

$$Y = \begin{bmatrix} y(k_i+1|k_i) & y(k_i+1|k_i) & \cdots & y(k_i+N_p|k_i) \end{bmatrix}^T, \tag{23}$$

$$U = \begin{bmatrix} \Delta u(k_i) & \Delta u(k_i+1) & \cdots & \Delta u(k_i+N_c-1) \end{bmatrix}^T, \tag{24}$$

$$F = \begin{bmatrix} CA \\ CA^2 \\ \vdots \\ CA^{N_p} \end{bmatrix}, \quad \phi = \begin{bmatrix} CB & 0 & \cdots & 0 \\ CAB & CA & \cdots & 0 \\ \vdots & \vdots & \cdots & 0 \\ CA^{N_p-1} & CA^{N_p-1} & \cdots & CA^{N_p-N_c} \end{bmatrix}. \tag{25}$$

Let $r(k)$ be the reference signal of the plant. The objective of GPC is to calculate an optimal vector U that minimize the error between the reference and the predicted plant outputs. Let $R_s \in \Re^{N_p \times 1}$ be a vector that contains the references of the predicted responses that composes Y. It is considered that R_S is constant inside the prediction window (the set of predictions) [22]. Equation (26) defines the reference vector R_s according to [22] :

$$R_S^T = \underbrace{\begin{bmatrix} 1 & 1 & \cdots, 1 \end{bmatrix}}_{N_p} r(k_i). \tag{26}$$

The cost function J, which reflects the control system performance, is defined in [22] as:

$$J = (R_S - Y)^T(R_S - Y) + U^T\overline{R_w}U, \quad \overline{R_w} = r_w I_c, \tag{27}$$

Preprints (www.preprints.org) | NOT PEER-REVIEWED | Posted: 2 December 2020 doi:10.20944/preprints202012.0045.v1

where $I_c \in \Re^{N_c \times N_c}$ is an identity matrix, while r_w is a tuning parameter used to control the magnitude of U [22]. The optimal solution of (27) makes $\frac{\partial J}{\partial U} = 0$ [22]:

$$\frac{\partial J}{\partial U} = -2\phi^T(R_S - Fx(k_i)) + 2(\phi^T\phi + \overline{R_w})U = 0. \tag{28}$$

By replacing (22) into (28) and after mathematical manipulations, the optimal solution U is [22]:

$$U = (\phi^T\phi + \overline{R_w})^{-1}\phi^T(R_S - Fx(k_i)). \tag{29}$$

According to receding horizon approach, only the first element of the optimal control trajectory, i.e., $\Delta u(k_i)$, is used as control law. Thus:

$$\begin{aligned} \Delta u(k_i) &= \overbrace{\begin{bmatrix} 1 & 0 & \cdots 0 \end{bmatrix}}^{N_c}(\phi^T\phi + \overline{R_w})^{-1}(\phi^T R_S r(k_i) - \phi^T Fx(k_i)) \\ &= K_y r(k_i) - K_{mpc}x(k_i), \end{aligned} \tag{30}$$

where K_y is the first element of $\phi^T\phi + \overline{R_w})^{-1}(\phi^T R_S)$ and K_{mpc} is the first line of $\phi^T\phi + \overline{w})^{-1}(\phi^T Fx(k_i))$. The gain vector K_{mpc} can be expressed as $K_{mpc} = [K_x\ K_y]$, where $K_y \in \Re^{1\times 1}$ is the last element of K_{mpc}, while $K_x \in \Re^{n\times 1}$. Based on (30) and the definition of $x(k)$ in (17), it is possible to prove [22]:

$$\Delta u(k_i) = K_y(r(k_i) - y(k_1) - K_x\Delta x_m(k_i). \tag{31}$$

The closed-loop GPC system described in [22] can be described as shown in Figure 2, where z^{-1} block indicates the discrete delay operator, $1 - z^{-1}$ is the discrete transfer function equivalent to the Δ operator, while $\frac{1}{1-z^{-1}}$ corresponds to the discrete-time integrator. The plant input is obtained by integrating $\Delta u(k_i)$ in (31).

3. Proposed RDC System based on SOD-GPC

3.1. Second Order Difference GPC (SOD-GPC)

According to the internal model principle, if the plant has no integrator, then the controller must have two embedded integrators in order to track ramp references [36]. However, the conventional GPC approach in [22] only has one embedded integrator. Besides, the cost function of the GPC described in (27) considers that the prediction window reference vector (R_S) is constant within the prediction window [22]. However, the reference vector defined in (26) is not constant when the plant reference $r(k)$ is a ramp signal.

In [39] was proposed an adaptation of the GPC algorithm for track reference tracking. This approach is based on the application of the second-order difference operator in (4) to create an

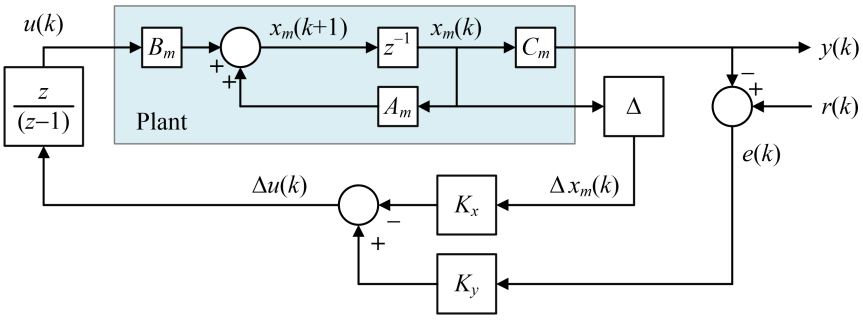

Figure 2. Conventional Generalized Predictive Control described in [22].

Preprints (www.preprints.org) | NOT PEER-REVIEWED | Posted: 2 December 2020 doi:10.20944/preprints202012.0045.v1

augmented model with two embedded integrators and whose output is the tracking error. In order to simplify the notation, the GPC approach in [39] will be called as second-order difference GPC (SOD-GPC) in this paper.

Applying the second-order difference operator into (8), and as this operator is linear, yields:

$$\Delta^2 x_m(k+1) = C_m A_m \Delta^2 x_m(k) + C_m B_m \Delta^2 u(k). \tag{32}$$

Let $e(k)$ be the tracking error:

$$e(k) = r(k) - y(k). \tag{33}$$

Hence

$$e(k+1) = r(k+1) - y(k+1). \tag{34}$$

Applying the first-order difference operator into (16), (33) and (34) yields [39]:

$$\Delta e(k) = \Delta r(k) - \Delta y(k), \tag{35}$$

$$\Delta e(k+1) = \Delta r(k+1) - \Delta y(k+1), \tag{36}$$

$$\begin{aligned} \Delta y(k+1) &= \Delta \left[y(k) + C_m A_m \Delta x_m(k) + C_m B_m \Delta u(k) \right] \\ &= \Delta y(k) + C_m A_m \Delta^2 x_m(k) + C_m B_m \Delta^2 u(k). \end{aligned} \tag{37}$$

On the other hand, let $r(k) = \alpha k + \beta$ be the ramp reference signal. Observe that $\Delta r(k) = r(k) - r(k-1) = \alpha$. Besides, $\Delta r(k+1) = r(k+1) - r(k) = \alpha$. Therefore:

$$\Delta r(k+1) = \Delta r(k). \tag{38}$$

Replacing (35), (37) and (38) into (36), yields

$$\begin{aligned} \Delta e(k+1) &= \Delta r(k) - \left[\Delta y(k) + C_m A_m \Delta^2 x_m(k) + C_m B_m \Delta^2 u(k) \right] \\ &= \Delta e(k) - C_m A_m \Delta^2 x_m(k) - C_m B_m \Delta^2 u(k). \end{aligned} \tag{39}$$

Observe that $\Delta e(k+1) = e(k+1) - e(k)$. Hence:

$$e(k+1) = e(k) + \Delta e(k+1). \tag{40}$$

Replacing (39) into (40), yields:

$$\begin{aligned} e(k+1) &= e(k) + \Delta e(k+1) \\ &= e(k) + \Delta e(k) - C_m A_m \Delta^2 x_m(k) - C_m B_m \Delta^2 u(k). \end{aligned} \tag{41}$$

The augmented model proposed defined in (42) is obtained from (32), (39) and (41) [39]:

$$\begin{aligned} x(k+1) &= Ax(k) + B\Delta^2 u(k), \\ \text{Output: } e(k) &= Cx(k), \end{aligned} \tag{42}$$

where

$$x(k) = \begin{bmatrix} \Delta^2 x_m(k) \\ \Delta e(k) \\ e(k) \end{bmatrix}, \quad A = \begin{bmatrix} A_m & o_o^T & o_o^T \\ -C_m A_m & 1 & o_o^T \\ -C_m A_m & 1 & 1 \end{bmatrix}, \quad B = \begin{bmatrix} B_m \\ -C_m B_m \\ -C_m B_m \end{bmatrix}, \tag{43}$$

$$C = \begin{bmatrix} o_o & 0 & 1 \end{bmatrix}.$$

Preprints (www.preprints.org) | NOT PEER-REVIEWED | Posted: 2 December 2020 doi:10.20944/preprints202012.0045.v1

Observe that the input and the output of (42) are $\Delta^2 u(k)$ and $e(k)$, respectively. In [39], the prediction window is composed by the predicted tracking errors $e(k_i+1|k_i), e(k_i+2|k_i), \cdots, e(k_i+N_p|k_i)$, while the future control trajectory is $\Delta^2 u(k_i), \Delta^2 u(k_i+1), \cdots, \Delta^2 u(k_i+N_c-1)$. Thus, the vector with the predicted response (Y_a) and the vector with the future control signals (U_a) for the SOD-GPC system proposed in [39] are defined as follows:

$$Y_a = \begin{bmatrix} e(k_i+1|k_i) & e(k_i+1|k_i) & \cdots & e(k_i+N_p|k_i) \end{bmatrix}^T, \tag{44}$$

$$U_a = \begin{bmatrix} \Delta^2 u(k_i) & \Delta^2 u(k_i+1) & \cdots & \Delta^2 u(k_i+N_c-1) \end{bmatrix}^T. \tag{45}$$

The proposed augmented model in (42) has a similar structure of the GPC augmented model in (17). Thus, it is possible to apply the method defined in (22) to predicted the tracking error (the outputs of the augmented model in (42):

$$Y_a = Fx(k_i) + \phi U_a, \tag{46}$$

where F and ϕ are defined in (25) but using the matrices A, B and C in (43).

Observe that the desired values of the predicted errors that composes Y_a is zero. Therefore, the reference vector is a set of zeros, i.e., $R_S = 0$, which is constant. As a result, the optimal solution U_a for SOD-GPC is obtained through replacing Y, U and R_S by Y_a, U_a and 0 into (27), (28) and (29) [39]:

$$J = Y_a^T Y_a + U_a^T \overline{R_w} U_a, \tag{47}$$

$$\frac{\partial J}{\partial U_a} = 2\phi^T F x(k_i) + 2(\phi^T \phi + \overline{R_w}) U_a = 0, \tag{48}$$

$$U_a = -(\phi^T \phi + \overline{R_w})^{-1} \phi^T F x(k_i). \tag{49}$$

Furthermore, the first element of U_a, i.e., $\Delta^2 u(k_i)$ is used to get the control law of the SOD-GPC, according to the receding horizon approach:

$$\Delta^2 u(k_i) = -\overbrace{\begin{bmatrix} 1 & 0 & \cdots 0 \end{bmatrix}}^{N_c} (\phi^T \phi + \overline{R})^{-1} \phi^T F x(k_i). \tag{50}$$

The plant input is obtained by integrating $\Delta^2 u(k_i)$ in (50) twice. Figure 3 shows the structure of the SOD-GPC system described in [39]. The dynamics of the control system depends on the tuning of N_p, N_c and $\overline{R_w}$.

$$\Delta u(k_i) = \Delta^2 u(k_i) + \Delta u(k_i - 1), \quad u(k_i) = \Delta u(k_i) + u(k_i - 1). \tag{51}$$

Let $G(z)$ and $G_a(z)$ be the discrete transfer functions of the plant and the SOD-GPC augmented model. It is proved in [39]:

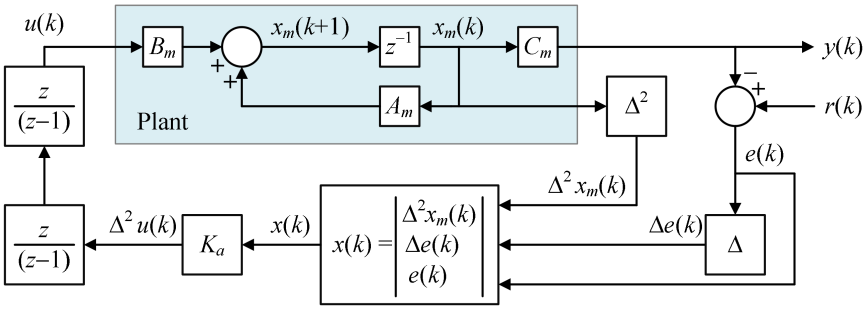

Figure 3. Schematic of the Second-Order Difference GPC system (SOD-GPC).

Preprints (www.preprints.org) | NOT PEER-REVIEWED | Posted: 2 December 2020 doi:10.20944/preprints202012.0045.v1

$$G_a = -\left[\frac{z}{z-1}\right]^2 G(z). \tag{52}$$

Equation (52) proves that the augmented model in (42) has two embedded integrators, when the plant has no zeros at $z = 1$. Hence, the SOD-GPC can asymptotically track ramp references [39].

3.2. Proposed GPC-Based ATO

Figure 4 shows the structure of the proposed ATO based on SOD-GPC. Let consider that the excitation signal is generated by the RDC. Thus, the value of this signal is known. Let $t = k.t_s$, where t is the discretized time, t_s is the sampling time, while k denotes the k-th sample. Let $\theta(k) = \theta(kt_s)$ and $\theta_e(k) = \theta_e(kt_s)$ be the actual and the estimated angle. Thus the resolver signals in (1), (2) and (3) can be discretized as follows:

$$\begin{aligned} v_e(k) &= a_r cos(\omega_r t_s k) = a_r cos(\omega_{rs} k), && (53)\\ v_s(k) &= k_r v_e(k) sin(\theta(k)), && (54)\\ v_c(k) &= k_r v_e(k) cos(\theta(k)), && (55) \end{aligned}$$

where $\omega_{rs} = \omega_r t_s$. According to (53), (54), (55) and Figure 4, the term $g(k)$ is

$$\begin{aligned} g(k) &= \frac{2}{k_r a_r^2}\left[v_s(k)cos(\theta_e(k)) - v_c(k)sin(\theta_e(k))\right] v_e(k) && (56)\\ &= \frac{2}{a_r^2}\left[sin(\theta(k))cos(\theta_e(k)) - cos(\theta(k))sin(\theta_e(k))\right] v_e^2(k)\\ &= 2sin(\theta(k) - \theta_e(k))cos^2(\omega_{rs}k)\\ &= sin(\theta(k) - \theta_e(k))\left[1 + cos(2\omega_{rs}k)\right]\\ &= sin(e_\theta(k)) + sin(e_\theta(k))cos(2\omega_{rs}k), \end{aligned}$$

where $e_\theta(k) = \theta(k) - \theta_e(k)$ is the angle estimation error. Assuming that $e_\theta(k) \approx 0$, then $sin(e_\theta(k)) \approx e_\theta(k)$. Thus (56) is rewritten as follows:

$$g(k) \approx e_\theta(k) + e_\theta(k)cos(2\omega_{rs}k). \tag{57}$$

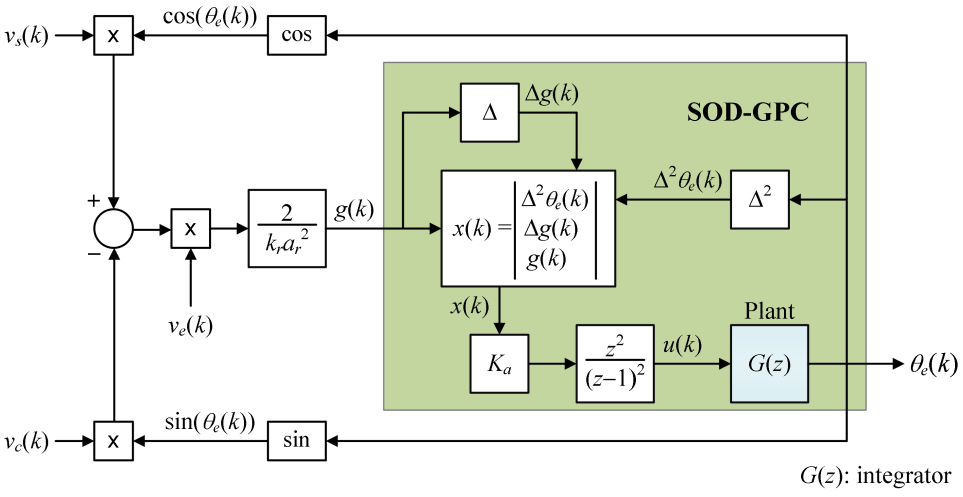

Figure 4. Proposed ATO based on SOD-GPC.

Preprints (www.preprints.org) | NOT PEER-REVIEWED | Posted: 2 December 2020 doi:10.20944/preprints202012.0045.v1

Let $h(k)$ be the impulse response of the ATO. As the SOD-GPC is a linear system, it is possible to apply the superposition principle in order to analyze the ATO response: the estimated angular position (the ATO output) is the summation of the responses produced by $e_\theta(k)$ and $e_\theta(k)cos(2\omega_{rs}k)$:

$$\begin{aligned} \theta_e(k) &= h(k) * g(k) \\ &= h(k) * [e_\theta(k) + e_\theta(k)cos(2\omega_{rs}k)] \\ &= h(k) * e_\theta(k) + h(k) * [e_\theta(k)cos(2\omega_{rs}k)], \end{aligned} \tag{58}$$

where * denotes convolution. Through frequency shifting property, it is possible to prove that the term $e_\theta(k)cos(2\omega_{rs}k)$ is a high frequency signal, while the ATO acts as a low-pass filter that reject high-frequency signals [18]. As a result, the effect of the signal $e_\theta(k)cos(2\omega_{rs}k)$ in the angle estimation will be rejected by the ATO:

$$h(k) * [e_\theta(k)cos(2\omega_{rs}k)] \approx 0. \tag{59}$$

Replacing (59) into (58) yields:

$$\theta_e(k) \approx h(k) * e_\theta(k). \tag{60}$$

Equation (60) states that the estimated angle mainly depends on the term $e_\theta(k)$. In consequence, the ATO can be projected only considering the existence of $e_\theta(k)$. Thus, the ATO can be approximated as the closed-loop system in Figure 5, where the reference is $\theta(k)$, the output is $\theta_e(k)$ and the SOD-GPC is the controller that reduce the error $e_\theta(k)$. Besides, the plant whose output will be defined by the SOD-GPC algorithm is the integrator represented by $G(z)$ in Figure 5. The discrete-time model of the integrator is described through (8) and (9), where $A_m = 1$, $B_m = t_s$, $C_m = 1$ and $y(k) = x_m(k) = \theta_e(k)$. Besides, the closed-loop error ($e(k)$) is the angle estimation error, i.e., $e(k) = e_\theta(k)$. Replacing these terms into (43) yields:

$$x(k) = \begin{bmatrix} \Delta^2\theta_e(k) \\ \Delta e(k) \\ e(k) \end{bmatrix}, \quad A = \begin{bmatrix} 1 & 0 & 0 \\ -1 & 1 & 0 \\ -1 & 1 & 1 \end{bmatrix}, \quad B = \begin{bmatrix} t_s \\ -t_s \\ -t_s \end{bmatrix}, \quad C = \begin{bmatrix} 0 & 0 & 1 \end{bmatrix}. \tag{61}$$

The matrices A, B and C in (61) must be used to obtain the gain matrix K_a and the control law according to (25), (50) and (51). It is required the adequate tuning of the parameters N_p, N_c, and $\overline{R_w}$ to define the transient behavior of the ATO.

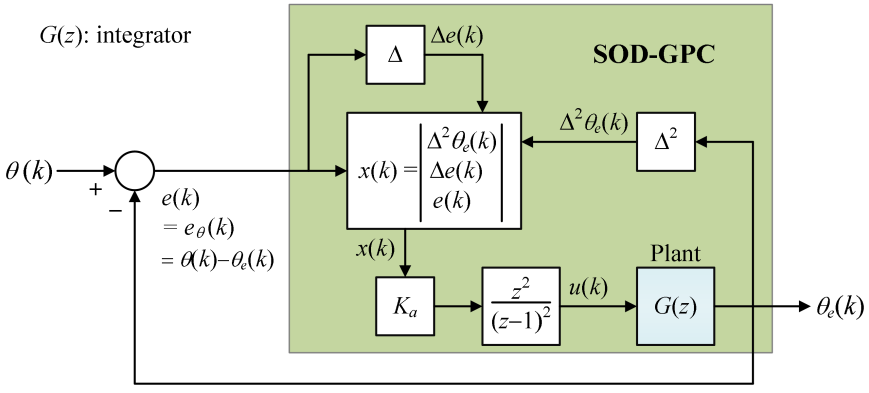

Figure 5. Simplified block diagram of the proposed ATO considering only the effect of $e_\theta(k)$ in the angle estimation.

Preprints (www.preprints.org) | NOT PEER-REVIEWED | Posted: 2 December 2020 doi:10.20944/preprints202012.0045.v1

4. Results

4.1. Simulation Results

A set of simulation tests were performed in SIMULINK to demostrate the performance of the proposed ATO. The sampling rate was set in 50 kHz. The parameters of the resolver sensor are listed in Table (1). The angular position correspond to the speed curve shown in Figure (6). The proposed ATO was tested considering different values of N_p, N_c and $\overline{R_w}$:

- Configuration 1: $N_p = 102, N_c = 2, \overline{R_w} = 0.01$,
- Configuration 2: $N_p = 120, N_c = 2, \overline{R_w} = 0.01$,
- Configuration 3: $N_p = 102, N_c = 10, \overline{R_w} = 0.01$.

The proposed approach was compared with the RDC described in [41]. The type-II tracking system shown in Figure 7 is used in [41] to estimate the angular position. The dynamics of that ATO depends on the eingenvalues of the matrix $M = \begin{bmatrix} 0 & 0 & 0 \\ -1 & 0 & 0 \\ 0 & 1 & 0 \end{bmatrix} - \begin{bmatrix} 0.5\,(k_r a_r)^2 \\ 0 \\ 0 \end{bmatrix} \underbrace{[k_0 - k_1 - k_2]}_{K}$. Ackermann formula can be used to get the matrix K in order to set the eigenvalues of M. In this paper, those eigenvalues were set in $-100 + j100$, $-100 - j100$, and -500.

For each ATO configuration, two tests were performed: without adding noise to the resolver outputs, and adding a noise (zero mean and 0.0002 variance) to the resolver outputs. Figures 8, 9, 10 and 11 show the angle estimation error for each simulation test.

Table 1. Simulation Parameters of the Resolver Sensor.

Parameters	Values
Excitation amplitude (a_r)	8 V
Excitation frequency (f_r)	2.5 kHz
Transformation ratio (k_r)	0.5

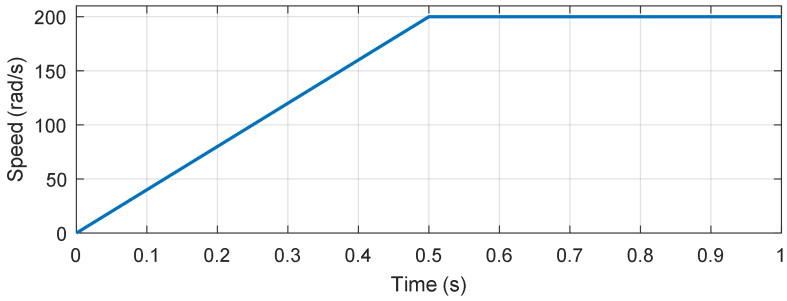

Figure 6. Speed curve used in the tests.

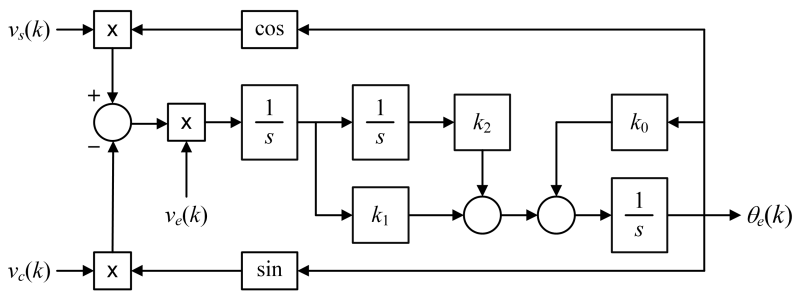

Figure 7. RDC system described in [41].

Preprints (www.preprints.org) | NOT PEER-REVIEWED | Posted: 2 December 2020 doi:10.20944/preprints202012.0045.v1

Table 2 shows the root mean square error (RMSE) and the error settling time (the time required for the error signal to achieve its steady-state value) for each simulation test. The errors without noise are negligible in all cases. However, it is possible to see that ATO in [41] has higher RMSE and settling time than the proposed approach. As a result, the proposed RDC system based on SDO-GPC has faster response and more robustness than the approach in [41].

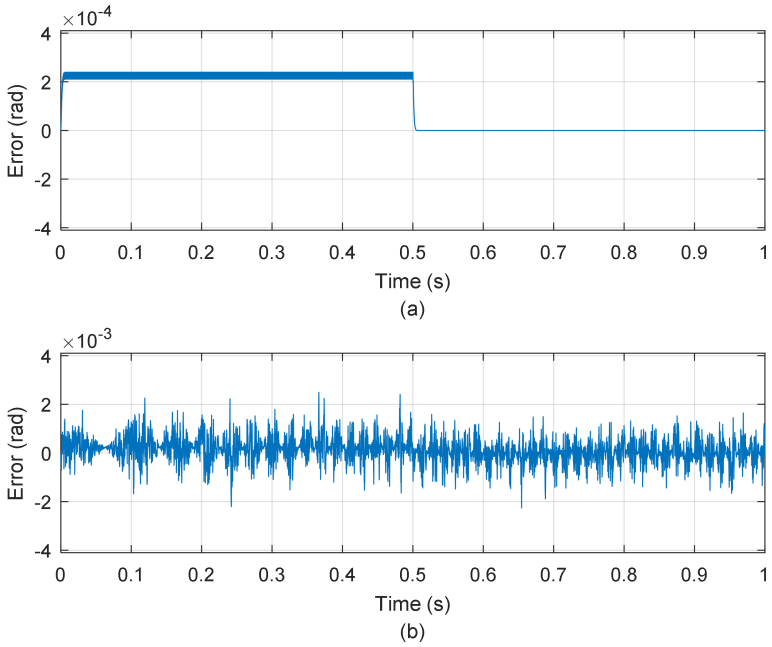

Figure 8. Simulation results for $N_p = 102, N_c = 2, \overline{R_w} = 0.01$. a) Without noise, b) With noise.

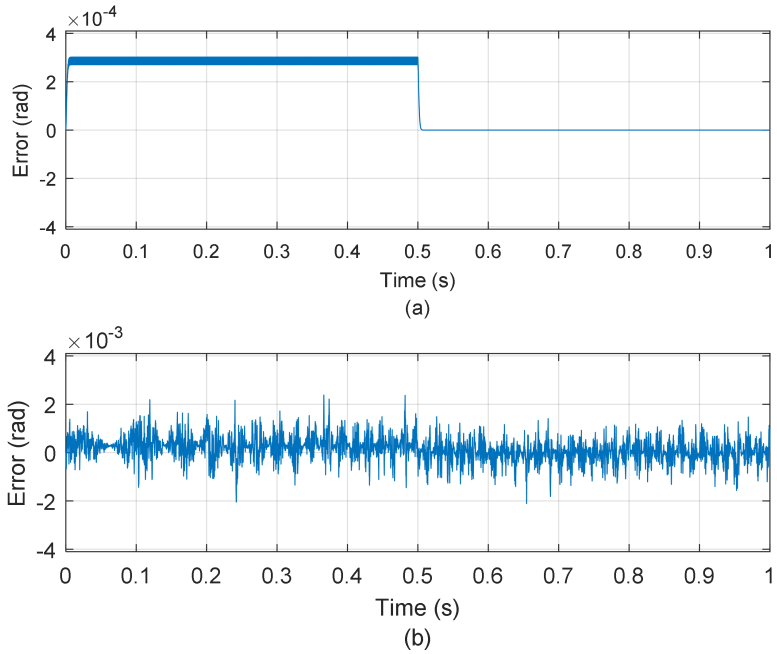

Figure 9. Simulation results for $N_p = 120, N_c = 2, \overline{R_w} = 0.01$. a) Without noise, b) With noise.

Preprints (www.preprints.org) | NOT PEER-REVIEWED | Posted: 2 December 2020 doi:10.20944/preprints202012.0045.v1

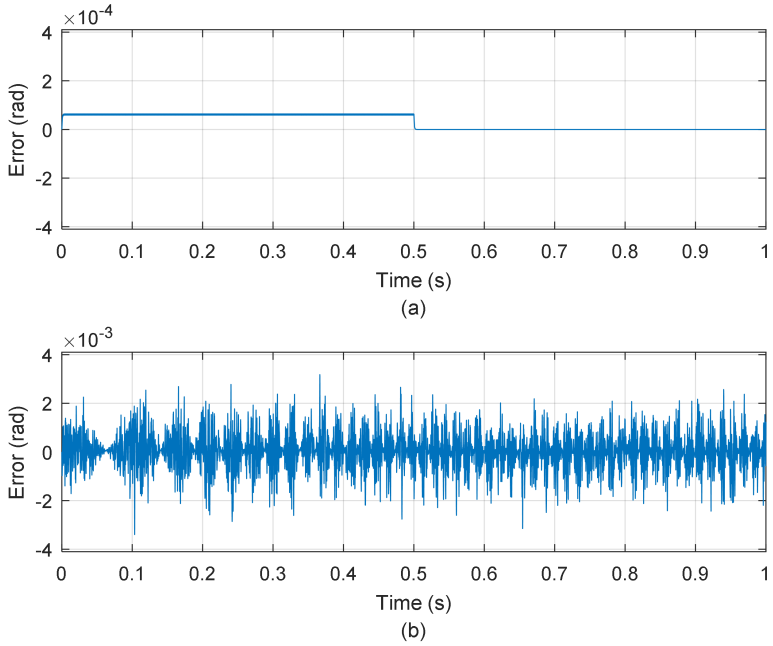

Figure 10. Simulation results for $N_p = 102, N_c = 10, \overline{R_w} = 0.01$. a) Without noise, b) With noise.

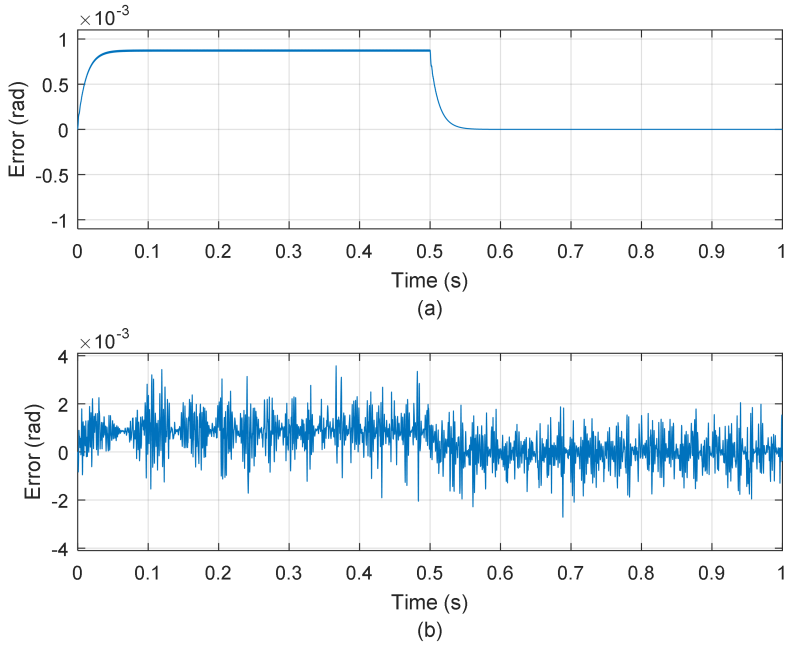

Figure 11. Simulation results for the ATO in [41]. a) Without noise, b) With noise.

Table 2. RMSE and Settling Time in the Simulation Tests.

Configuration	RMSE (without noise)	RMSE (with noise)	Settling Time (s)
$N_p = 102, N_c = 2, \overline{R_w} = 0.01$	0.16×10^{-3}	0.48×10^{-3}	4.90×10^{-3}
$N_p = 120, N_c = 2, \overline{R_w} = 0.01$	0.20×10^{-3}	0.47×10^{-3}	5.10×10^{-3}
$N_p = 102, N_c = 10, \overline{R_w} = 0.01$	0.04×10^{-3}	0.68×10^{-3}	2.10×10^{-3}
ATO in [41]	0.61×10^{-3}	0.88×10^{-3}	55.0×10^{-3}

Preprints (www.preprints.org) | NOT PEER-REVIEWED | Posted: 2 December 2020 doi:10.20944/preprints202012.0045.v1

4.2. Experimental Results

In order to test the proposed ATO, an experimental platform based on hardware-in-the-loop (HIL) was set up. The experimental setup shown in Figure 12 consists of a PC and the FPGA Development and Education Board DE2-115 of ALTERA (based on the FPGA EP4CE115F29C7). An Ethernet cable allows the communication between the FPGA board and the PC.

In the HIL testing method used in this paper, the resolver signals are generated through a SIMULINK block diagram in the PC. These signals are sent to the FPGA board through the Ethernet cable. The FPGA board receives these signals, estimates the angular position through the proposed ATO algorithm, and sends this estimation to the block diagram in the PC in order to calculate the angle estimation error. One advantage of using the HIL method is that the angular position in known in each instant. Thus, the angle estimation error can be calculated with accuracy. On the other hand, when a practical resolver is used, an additional angular position sensor with better accuracy (which is difficult to obtain) is required to get the actual angular position.

The proposed ATO was implemented in the FPGA board through a VHDL code, considering the same signal sampling frequency (50 kHz) and the SOD-GPC parameters used in the simulation tests. It was used 32-bits fixed-point data format in order to perform the arithmetic operations. However, the estimated angular position was represented using 40 bits (30 fractional bits) in order to do a better comparison between the actual and the estimated angle. The emulated resolver signals are the same as those used in the simulation tests.

Figures 13, 14 and 15 show the results for the HIL tests. In the tests without noise, it is possible to see a ripple in the angular position error during constant speed operation (from 0 s to 1 s). This ripple is produced by the limited number of bits used for the arithmetic operations. However, that ripple is negligible (that ripple has an amplitude less than $5 \times 10-5$ rad). Table (3) presents the RMSE and the settling time obtained in each HIL test. These values are similar to those obtained in simulations. The greater the value of N_c, the faster the ATO response but the greater the RMSE.

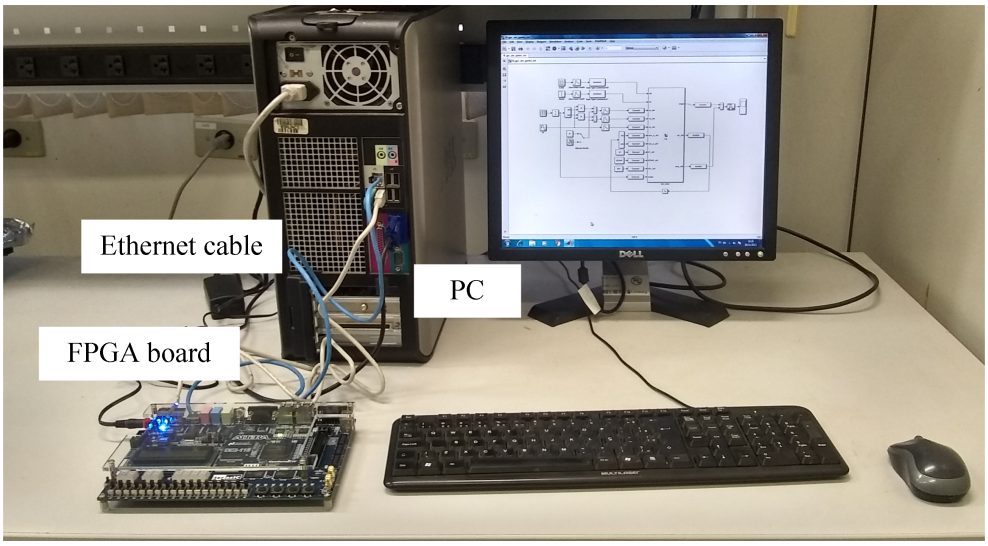

Figure 12. Experimental setup.

Table 3. RMSE and Settling Time in the Experimental HIL Tests.

Configuration	RMSE (without noise)	RMSE (with noise)	Settling Time (s)
$N_p = 102, N_c = 2, \overline{R_w} = 0.01$	0.18×10^{-3}	0.48×10^{-3}	5.50×10^{-3}
$N_p = 120, N_c = 2, \overline{R_w} = 0.01$	0.23×10^{-3}	0.47×10^{-4}	5.90×10^{-3}
$N_p = 102, N_c = 10, \overline{R_w} = 0.01$	0.06×10^{-3}	0.69×10^{-4}	3.90×10^{-3}

Preprints (www.preprints.org) | NOT PEER-REVIEWED | Posted: 2 December 2020 doi:10.20944/preprints202012.0045.v1

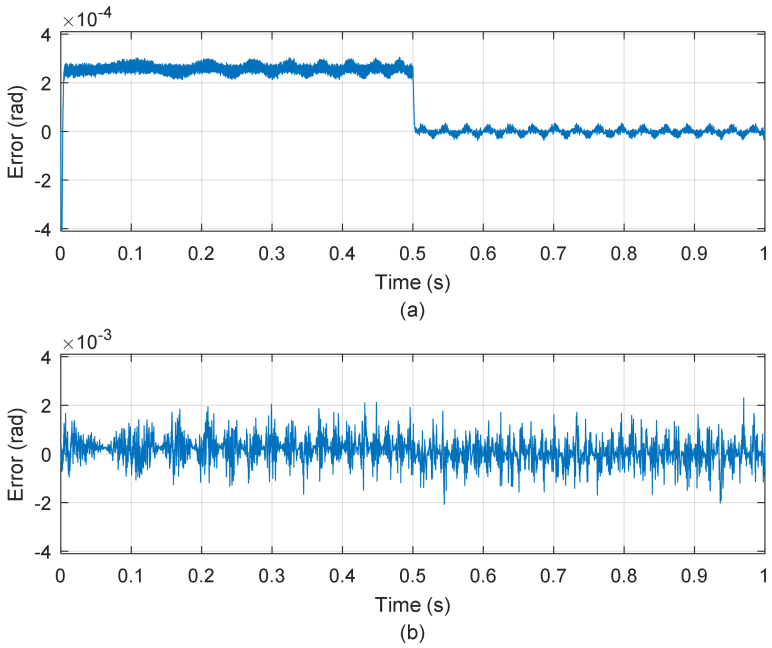

Figure 13. Experimental results for $N_p = 102$, $N_c = 2$, $\overline{R_w} = 0.01$. a) Without noise, b) With noise.

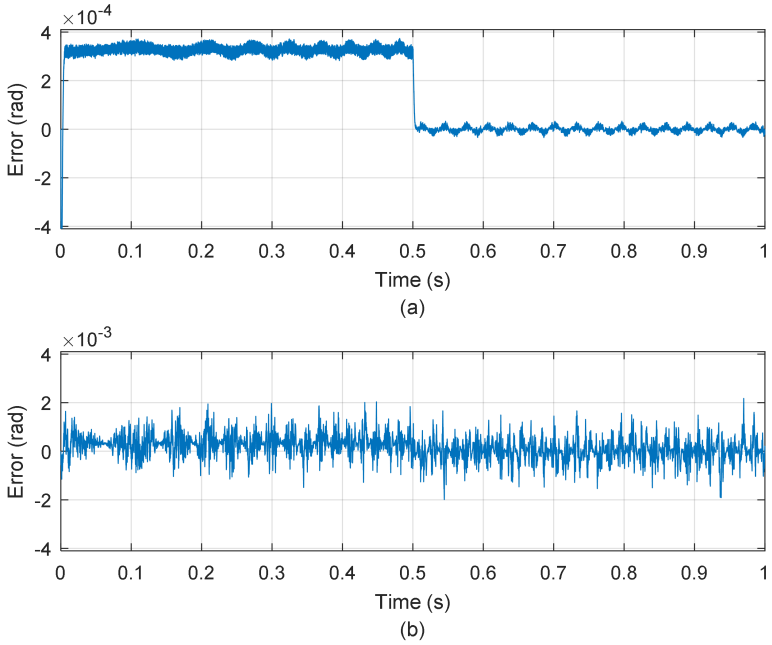

Figure 14. Experimental results for $N_p = 120$, $N_c = 2$, $\overline{R_w} = 0.01$. a) Without noise, b) With noise.

It was not possible to properly implement the ATO in Figure 7 in the FPGA using 32 bits fixed-point number representation. The main problem was the discretization of the integrators considering a sampling rate of 50 kHz. On the other hand, the SOD-GPC is a discrete-time control system, being easier to implement in a digital processor (no discretization is needed). As a result, the proposed RDC based on a SOD-GPC based ATO has a fast response, robustness against noise and it is suitable to be implemented in digital processors such as FPGAs.

Preprints (www.preprints.org) | NOT PEER-REVIEWED | Posted: 2 December 2020 doi:10.20944/preprints202012.0045.v1

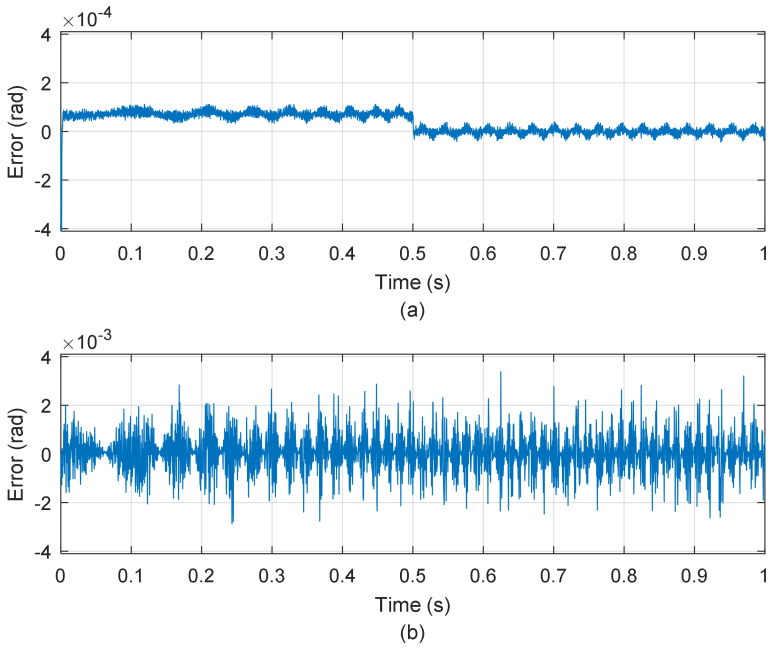

Figure 15. Experimental results for $N_p = 102$, $N_c = 10$, $\overline{R_w} = 0.01$. a) Without noise, b) With noise.

5. Conclusions

This paper presented a new angle tracking observer (ATO) based on second-order difference GPC system (SOD-GPC). The proposed ATO has a steady-state error that tends to zero during constant speed operation, a faster response and it is more robust than other ATOs. The GPC approach applied in this work is a discrete-time control system. Hence, the GPC structure suitable for its implementation in digital processor. Other ATOs, as in [41], are based on the discretization of continuous-time tracking systems. The discretization may reduce the performance of a control system. The dynamic behavior of the proposed ATO depends on the values of N_p, N_c and $\overline{R_w}$. As future work, an heuristic technique such as genetic algorithms will be used for the ATO tuning.

Author Contributions: G.G. and R.C. performed the simulation and experimental tests; T.E., G.G. and R.C. collaborated and supervised article writing; and T.E. did the theoretical analysis of the proposed system. All authors have read and agreed to the published version of the manuscript.

Funding: This research received no external funding.

Acknowledgments: Authors want to thank Federal Univesity of Mato Grosso do Sul for the support to this research.

Conflicts of Interest: The authors declare no conflict of interest.

References

1. Luo, P.; Tang, Q.; Jing, H.; Chen, X. Design and development of a self-calibration-based inductive absolute angular position sensor. *IEEE Sensors J.* **2019**, *19*, 135–142.
2. Zhang, Z.; Ni, F.; Dong, Y.; Guo, C.; Jin, M.; Liu, H. A novel absolute magnetic rotary sensor. *IEEE Trans. Ind. Electron.* **2015**, *62*, 4408–4419.
3. Jeon, N.; Lee, H. Integrated fault diagnosis algorithm for motor sensors of in-wheel independent drive electric vehicles. *Sensors* **2016**, *16*, 2106.
4. Mok, H.S.; Kim, S.H.; Cho; Y.H. Reduction of PMSM torque ripple caused by resolver position error. *Electron. Lett.* **2007**, *43*, 646 – 647.
5. Kovacs, I.; Iosub, A.; Ţopa, M.; Buzo, A.; Pelz, G. On the influence of angle sensor nonidealities on the torque ripple in PMSM systems — An analytical approach. In Proceedings of the 2016 13th International Conference

on Synthesis, Modeling, Analysis and Simulation Methods and Applications to Circuit Design (SMACD), Lisbon, Portugal, 27–30 June 2016; pp.
6. Hwang, M.-H.; Lee, H.-S.; Cha, H.-R. Analysis of Torque Ripple and Cogging Torque Reduction in Electric Vehicle Traction Platform Applying Rotor Notched Design. *Energies* **2018**, *11*, 3053.
7. Ni, Q.; Yang, M.; S. A. Odhano,; M. Tang,; P. Zanchetta,; X. Liu,; D. Xu, A new position and speed estimation scheme for position control of PMSM drives using low-resolution position sensors. *IEEE Trans. Ind. Appl.* **2019**, *55*, 3747–3758.
8. Tang, T.; Chen, S.; Huang, X.; Yang, T.; Qi, B. Combining load and motor encoders to compensate nonlinear disturbances for high precision tracking control of gear-driven gimbal. *Sensors* **2018**, *18*, 754.
9. Jin, C.-S.; Jang, I.-S.; Bae, J.-N.; Lee, J.; Kim, W.-H. Proposal of improved winding method for VR resolver. *IEEE Trans. on Magn.* **2015**, *51*, 1–4.
10. Gao, Z.; Zhou, B.; Hou, B.; Li, C.; Wei, Q.; Zhang, R. Self-calibration of nonlinear signal model for angular position sensors by model-based automatic search algorithm. *Sensors* **2019**, *19*, 2760.
11. Wang, K.; Wu, Z. Hardware-based synchronous envelope detection strategy for resolver supplied with external excitation generator. *IEEE Access* **2019**, *7*, 20801–20810.
12. Wang, S.; Kang, J.; Degano, M.; Buticchi, G. A resolver-to-digital conversion method based on third-order rational fraction polynomial approximation for PMSM control. *IEEE Trans. Ind. Electron.* **2019**, *66*, 6383–6392.
13. Idkhajine, L.; Monmasson, E.; Naouar, M.W.; Prata, A.; Boullaga, K.; Fully integrated FPGA-based controller for synchronous motor drive. *IEEE Trans. Ind. Electron.* **2009** *56*, 4006–4017.
14. Staebler, M.; Verma, A. *TMS320F240 DSP solution for obtaining resolver angular position and speed*; Texas Instrum. Inc., Dallas, TX, Appl. Rep. SPRA605A, Aug. 2017.
15. Abou Qamar, N.; Hatziadoniu, C.J.; Wang, H. Speed error mitigation for a DSP-based resolver-to-digital converter using autotuning filters. *IEEE Trans. Ind. Electron.* **2015**, *62*, 1134–1139.
16. Kaewjinda, W.; Konghirun, M. A. DSP - based vector control of pmsm servo drive using resolver sensor. In Proceedings of the 2006 IEEE Region 10 Conference (TENCON), Hong Kong, China, 14–17 November 2006; pp. 1–4.
17. Idkhajine, L.; Monmasson, E.; Naouar, M.W.; Prata, A.; Boullaga, K. Fully integrated FPGA-based controller for synchronous motor drive. *IEEE Trans. Ind. Electron.* **2009**, *56*, 4006–4017.
18. Garcia, R.C.; Pinto, J.O.P.; Suemitsu, W.I.; Soares, J.O. Improved demultiplexing algorithm for hardware simplification of sensored vector control through frequency-domain multiplexing. *IEEE Trans. Ind. Electron.* **2017**, *64*, 6538–6548.
19. Smidl, V.; Janous, S.; Peroutka Z.; Adam, L. Time-optimal current trajectory for predictive speed control of PMSM drive. In Proceedings of the 2017 IEEE International Symposium on Predictive Control of Electrical Drives and Power Electronics (PRECEDE), Pilsen, Czech Republic, 4–6 September 2017; pp. 83–88.
20. Moreno, J. C.; Espi Huerta, J. M. ; Gil, R. G.; Gonzalez, S. A. A robust predictive current control for three-phase grid-connected inverters. *IEEE Trans. Ind. Electron.* **2009**, *56*, 1993–2004.
21. Camacho, E. F.; Bordons, C. *Model Predictive Control*, 2nd ed.; Springer-Verlag London: London, 2004; pp. 13–124.
22. Wang, L. *Model Predictive Control System Design and Implementation Using Matlab®*; Springer-Verlag London: London, 2009; pp. 1–20.
23. Ruchika, N. R. Model predictive control: history and development. *Int. J. Eng.. Trends and Technol.* **2013**, *4*, 2600–2602.
24. Qin, S. J.; Badgwell, T. A. A survey of industrial model predictive control technology. In Proceedings of the 2016 European Control Conference (ECC), 29 June–1 July 2016, 2003; pp. 733–764.
25. Clarke, D.W.; Mohtadi, C.; Tuffs, P.S. Generalized predictive control - part I. the basic algorithm. *Automatica* **1987**, *23*, 137–148.
26. Clarke, D.W.; Mohtadi, C.; Tuffs, P.S. Generalized Predictive Control - Part II. Extensions and Interpretations. *Automatica* **1987**, *23*, 149–160.
27. Prajwowski, K.; Golebiewski, W.; Lisowski, M.; Abramek, K.F.; Galdynski, D. Modeling of working machines synergy in the process of the hybrid electric vehicle acceleration. *Energies* **2020**, *13*, 5818.
28. Wang, F.; Zhang, Z.; Mei, X.; Rodríguez, J.; Kennel, R. Advanced control strategies of induction machine: field oriented control, direct torque control and model predictive control. *Energies* **2018**, *11*, 120.

29. Gonçalves, P.; Cruz, S.; Mendes, A. Finite control set model predictive control of six-phase asymmetrical machines—an overview. *Energies* **2019**, *12*, 4693.
30. Nguyen, T.-T.; Yoo, H.-J.; Kim, H.-M.; Nguyen-Duc, H. Direct phase angle and voltage amplitude model predictive control of a power converter for microgrid applications. *Energies* **2018**, *11*, 2254.
31. Jin, N.; Pan, C.; Li, Y.; Hu, S.; Fang, J. Model predictive control for virtual synchronous generator with improved vector selection and reconstructed current. *Energies* **2020**, *13*, 5435.
32. Abdelrahem, M.; Hackl, C.M.; Rodríguez, J.; Kennel, R. Model reference adaptive system with finite-set for encoderless control of PMSGs in micro-grid systems. *Energies* **2020**, *13*, 4844.
33. Turley, C.; Jacoby, M.; Pavlak, G.; Henze, G. Development and evaluation of occupancy-aware hvac control for residential building energy efficiency and occupant comfort. *Energies* **2020**, *13*, 5396.
34. Bahramnia, P.; Hosseini Rostami, S.M.; Wang, J.; Kim, G.-J. Modeling and controlling of temperature and humidity in building heating, ventilating, and air conditioning system using model predictive control. *Energies* **2019**, *12*, 4805.
35. Estrabis, T.; Cordero, R.; Batista, E.; Andrea, C.; Grassi, M.A.S. Application of model predictive control in a resolver-to-digital converter. In Proceedings of the 2019 IEEE 15th Brazilian Power Electronics Conference and 5th IEEE Southern Power Electronics Conference (COBEP/SPEC), Santos, SP, Brazil, 1–4 Dec. 2019; pp. 1–6.
36. Dorf, R.C.; Bishop, R.H. *Modern Control Systems, 8th ed*; Addison Wesley Longman, Inc: Menlo Park, Ca. USA, 1998; pp. 662–666.
37. Belda, K.; Vosmik, D. Explicit generalized predictive control of speed and position of PMSM drives. *IEEE Trans. Ind. Electron.* **2016**, *63*, 3889–3896.
38. Maeder, U.; Morari, M. Offset-free reference tracking with model predictive control. *Automatica* **2010**, *46*, 1469–1476.
39. Cordero, R.; Estrabis, T.; Batista, E. A., Andrea, C. Q.; Gentil, G. Ramp-tracking generalized predictive control system based on second-order difference. *IEEE Trans. Circuits Syst. II, Exp. Briefs* **2020**, to be published. DOI: 10.1109/TCSII.2020.3019028.
40. Jerry, A. J. *Difference Equations with Discrete Transform Methods*; Springer Science+Business Media: Dordrecht, Netherlands, 1996; pp. 1–22.
41. Cordero, R.; Pinto, J.O.P.; Ono, I.E.; Fahed, H.D.S.; Brito, M. Simplification of the acquisition system for sensored vector control using resolver sensor based on fdm and current synchronous sampling. In Proceedings of the 2018 IEEE 4th Southern Power Electronics Conference (SPEC), Singapure, Singapure, 10-13 Dec. 2018; pp. 1–4.

Sample Availability: Samples of the compounds ..... are available from the authors.